

Contents lists available at [ScienceDirect](https://www.sciencedirect.com)

# Colloids and Surfaces A: Physicochemical and Engineering Aspects

journal homepage: [www.elsevier.com/locate/colsurfa](https://www.elsevier.com/locate/colsurfa)

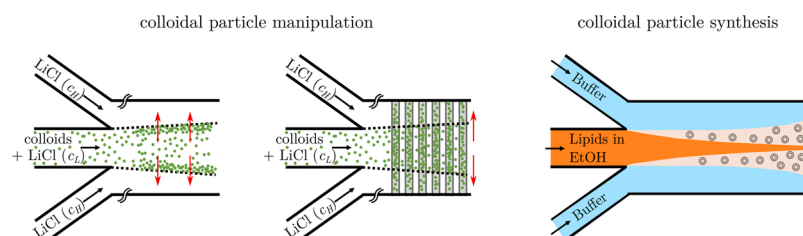
## Composite Norland Optical Adhesive (NOA)/silicon flow focusing devices for colloidal particle manipulation and synthesis

Naval Singh<sup>a,1</sup>, Adnan Chakra<sup>a</sup>, Goran T. Vladislavljević<sup>a</sup>, Cécile Cottin-Bizonne<sup>b</sup>,  
Christophe Pirat<sup>b</sup>, Guido Bolognesi<sup>a,\*</sup>

<sup>a</sup> Department of Chemical Engineering, Loughborough University, Loughborough LE11 3TU, United Kingdom

<sup>b</sup> Institut Lumière Matière, UMR5306 Université Claude Bernard Lyon 1 - CNRS, Université de Lyon, Villeurbanne Cedex 69622, France

### GRAPHICAL ABSTRACT



### ARTICLE INFO

**Keywords:**  
Microfabrication  
Microfluidics  
Flow focusing  
Liposomes  
Diffusiophoresis  
Nanoparticles  
NOA  
Silicon

### ABSTRACT

Microfluidic flow focusing devices are widely used to generate steep chemical concentration gradients at the interface between miscible or partially miscible streams. In this study, first we present an optimised protocol for the manufacturing of composite flow focusing devices, consisting of a micropatterned layer of Norland Optical Adhesive (NOA) glue bound to flat or microgrooved silicon substrates. Then, three different applications of these devices are demonstrated, namely (i) particle spreading and focusing in continuous flows past flat substrates, (ii) particle accumulation within the dead-end cavities of microgrooved substrates and (iii) synthesis of nano-sized liposomes. Colloidal particle spreading, focusing and accumulation were achieved through diffusiophoresis transport induced by salt concentration gradients at the interface between electrolyte streams. Epi-fluorescence microscopy was adopted to characterise the spatio-temporal distribution of silica and polystyrene nanoparticles in the devices with flat or microgrooved surfaces. The effects of particle zeta potential and groove thickness on particle dynamics were investigated. 1,2-di-(9Z-octadecenoyl)-sn-glycero-3-phosphocholine (DOPC) liposomes were generated by hydrodynamic focusing and characterised via dynamic light scattering. Liposome populations with controlled narrow size distributions could be achieved by adjusting the flow rate conditions in the devices. This work demonstrates that composite NOA/silicon flow junction devices offer a competitive alternative to conventional PDMS chips and can support a wide range of microfluidic applications, including nanoparticle synthesis, characterisation and filtration, drug encapsulation and biochemical analysis.

\* Corresponding author.

E-mail address: [g.bolognesi@lboro.ac.uk](mailto:g.bolognesi@lboro.ac.uk) (G. Bolognesi).

<sup>1</sup> Present Address: Manchester Centre for Nonlinear Dynamics, Department of Physics and Astronomy, University of Manchester, Manchester M13 9PL, United Kingdom

<https://doi.org/10.1016/j.colsurfa.2022.129808>

Received 30 April 2022; Received in revised form 24 July 2022; Accepted 25 July 2022

Available online 27 July 2022

0927-7757/© 2022 The Authors. Published by Elsevier B.V. This is an open access article under the CC BY license (<http://creativecommons.org/licenses/by/4.0/>).

## 1. Introduction

Microfluidic devices play a pivotal role in many physical, chemical, biological and engineering applications relevant to both research and commercial use [1]. The choice of the device material and fabrication method is a crucial step that can determine the overall viability of the proposed microfluidic application. The first generation of microfluidic chips were prepared in glass and silicon, as these materials were traditionally used by the molecular analysis and microelectronic industries [2–4]. Due to their many key advantages, as excellent solvent compatibility, high thermoconductivity, good surface stability, high elastic modulus and stable electroosmotic mobility, glass and silicon are still widely used in microfluidic research [5–9]. Since silicon is transparent to infrared but not to visible light, glass devices are usually preferred when optical access to the flow is required, such as in fluorescence detection or fluid imaging. Alternatively, silicon microchannels can be bound to a transparent material (glass or polymer), thereby resulting in a composite device with optical access from one side only.

Over the past decades, many pioneering studies have introduced microfluidic fabrication methods using polymers and some of these methods (e.g. hot embossing, injection moulding) are relatively inexpensive and more easily scalable for large production [10,11,47]. In laboratory settings, the most accustomed polymer is certainly polydimethylsiloxane (PDMS) because of its many excellent physical and chemical properties. PDMS devices have good chemical and thermal stability, are easy to functionalise via physical or chemical surface treatments, are optically transparent, gas permeable, mechanically resistant, and soft enough to allow the integration of active flow control elements (e.g. valves and pumps). Also, the numerous PDMS-based soft-lithography techniques, developed over the years [12,13], made this elastomeric polymer a standard tool of many microfluidic research laboratories. Since the seminal work by Bartolo et al. [14], optically transparent and chemically-resistant photocurable polymers, such as Norland Optical Adhesive (NOA) glues, have been increasingly used for microfluidic device fabrication due to their excellent optical transparency, chemical resistance to many organic solvents, impermeability to gases and water vapour, and relatively high elastic modulus that prevents channel deformation under high pressure flows. NOA devices can be fabricated via a soft-lithography process, called microfluidic sticker technique [14], which also allows the manufacturing of composite devices made of NOA and another gas-impermeable substrate (e.g. glass, silicon). Notably, the NOA components of these composite devices can be dissolved in chlorinated solvents, thereby enabling the recovery of the other substrates after device use.

Flow focusing channel design, where an inner channel meets two outer channels at a junction, has been extensively used in several microfluidic applications [15–17]. When two immiscible streams (like water and oil) meet at a flow focusing junction, the high shear stress can mediate the interfacial tension-driven destabilisation of the liquid-liquid interface and lead to the controlled production of emulsion droplets and microparticles [17,18]. Alternatively, when the two streams are miscible or partially miscible, the flow focusing configuration can be exploited to create narrow diffusion layers with steep chemical concentration gradients at the interface between the two streams. The mixing of chemicals in the diffusion layer can trigger chemical reactions or physico-chemical responses, leading to the synthesis of nanoparticles under continuous flow settings [19,20]. For instance, hydrodynamic flow focusing has been adopted to produce narrow-sized populations of liposomes, micelles and metallic nanoparticles, encapsulating drugs or other active ingredients [21–24]. Furthermore, chemical gradients in flow focusing devices can be exploited to induce the spontaneous migration of colloidal particles along the streamlines of the chemical gradient field, a phenomenon referred to as diffusiophoresis [25,26]. By relying on this phoretic transport mechanism, flow focusing devices generating salt concentration gradients have been developed to achieve colloidal particle spreading, focusing, filtration and accumulation

[27–29].

In this study, we report the optimised protocol for the fabrication of composite NOA flow focusing devices bound to flat and microgrooved silicon substrates. Three different applications of these devices are demonstrated, namely (i) particle spreading and focusing on flat substrates, (ii) particle accumulation within the grooves of microstructured substrates and (iii) synthesis of liposomes with controlled narrow size distributions. This is the first study to investigate particle spreading and liposome synthesis in composite NOA/silicon flow focusing devices with flat walls, and to analyse the effects of particle chemistry (i.e., polystyrene and silica) and groove thickness on the solute-driven accumulation process within microgrooved channels. Our results demonstrate the potential of NOA flow focusing devices as a valuable tool for supporting fundamental research in physics and chemistry as well as underpinning a wide range of microfluidic applications, such as nanoparticle synthesis and characterisation, drug encapsulation and bioanalysis. Hence, this work will further encourage the interdisciplinary uptake of NOA microfluidics by the scientific community and consolidate its role as a competitive alternative to conventional PDMS microfluidics.

## 2. Experimental

### 2.1. Materials

Negative photoresist SU-8–2050 (MicroChem Corp.) and photoresist developer (EC-Solvent) were purchased from A-Gas Electronic Materials. Polydimethylsiloxane (PDMS) (Momentive RTV615 A+B-Kit, base + curing agent) was purchased from Techsil, and the photoreactive adhesive Norland Optical Adhesive 81 (NOA-81) from Norland Products Inc. The silicon microgrooved substrates were fabricated via Deep Reactive Ion Etching (DRIE) by MIMENTO (Microfabrication for MEchanics, Nanosciences, Thermal and Optics) technology centre, hosted by FEMTO-ST Institut in Besançon, France. The substrates had transverse grooves, 24  $\mu\text{m}$  thick, 45  $\mu\text{m}$  deep and 2 mm wide, evenly spaced 32  $\mu\text{m}$  apart over a 4 cm long region. The rectangular flat silicon surfaces, used for the fabrication of the flat microchannels, were manually cut from four inch diameter silicon wafers, purchased from Inseto.

The fluorescent silica nanobeads (0.05 % solids w/v) were purchased from the Kisker Biotech GmbH & Co.KG company, and the fluorescent polystyrene nanobeads (FluoSpheres™, 1.02 % solids w/v) were purchased from Thermo Fisher Scientific. All colloidal nanobeads have a nominal diameter of 200 nm. The lithium chloride salt (LiCl, 99 %) was purchased from Acros Organics. TRIS hydrochloride, ethylenediaminetetraacetic acid (EDTA) (98.5 %), HEPES (99.5 %), ethanol and 1,2-di-(9Z-octadecenoyl)-sn-glycero-3-phosphocholine (DOPC) were purchased from Sigma-Aldrich. All aqueous solutions were prepared using DI water of resistivity 18.2 M $\Omega\text{cm}$  from an Ultrapure Milli-Q grade purification system (Millipore, USA). The chlorinated solvent, dichloromethane (anhydrous,  $\geq 99.8$  %) chloroform (anhydrous,  $\geq 99$  %), methanol (anhydrous, 99.8 %) and ammonium hydroxide, used for recovery of the microgrooved substrate, were purchased from Sigma-Aldrich.

### 2.2. Particle characterisation

Dynamic light scattering and electrophoretic light scattering measurements were performed to determine average particle size and zeta potential of colloidal particles, respectively. A Delsa™ Nano Zeta Potential and Submicron Particle Size Analyzer by Beckman Coulter provided an average particle size of silica nanoparticles of  $205 \pm 8$  nm and a zeta potential of  $-41.7 \pm 4$  mV in 1 mM TRIS buffer (pH=9). Polystyrene particles were characterised in 0.1 mM LiCl solution with a Malvern ZetaSize Nano ZS, providing an average particle size of  $207 \pm 7$  nm and a zeta potential of  $-58.5 \pm 1$  mV. Size distribution of the liposomes, manufactured in the microfluidic devices, were also measured

with the Malvern ZetaSizer Nano ZS. Note that for zeta potential measurements the instruments provided the zeta potential values calculated according to the Smoluchowski's theory for which the Debye length is much smaller than the particle size. The zeta potential values were corrected to account for the finite size of the Debye length according to Henry's model [30].

### 2.3. Microfabrication

SU-8 masters were fabricated via contact printing photolithography

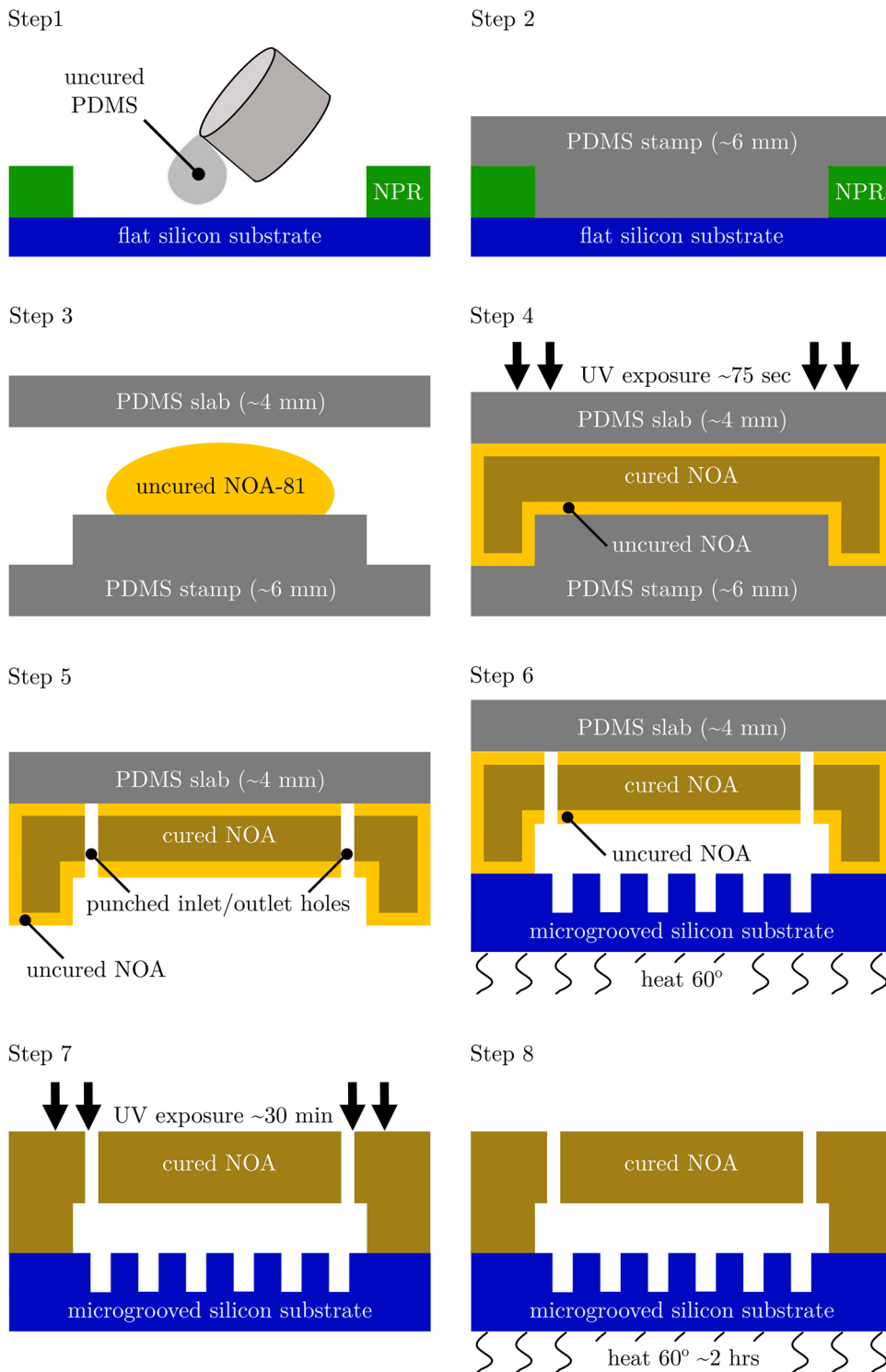


**Fig. 1.** Protocol for the fabrication of a NOA-81 microchannel on a microgrooved silicon substrate via microfluidic sticker technique. Steps 1–2: fabrication of a PDMS stamp, ca. 6 mm in thickness, via replica moulding from a photolithographically patterned negative photoresist (NPR). Step 3: spreading of a NOA-81 drop between the PDMS stamp and a PDMS slab (ca. 4 mm in thickness). Step 4: partial curing of the NOA-81 microchannel imprint via UV exposure. Step 5: removal of the PDMS stamp and punching of the inlet/outlet holes. Step 6: deposition of the NOA-81 microchannel on a microgrooved silicon substrate heated on a hot plate. Step 7–8: adhesion of the NOA-81 microchannel on the silicon substrate via UV exposure and heating.

## 2.4. Fluorescence microscope analysis

Syringe pumps (Harvard Pump 11 Elite) were used to inject the desired solutions within the microfluidic devices. For particle manipulation experiments, epi-fluorescence images of the particles were acquired via a Nikon Eclipse TE-300 inverted microscope, fitted with a led lamp (CoolLED pE-300), a CMOS camera (Ximea MQ013MG-ON) and a 10x (0.25 NA) objective. The excitation/emission peaks of the particles are 485/510 nm for silica beads and 542/612 nm for polystyrene beads. A filter cube (Nikon B-2A) with 450–490 nm excitation bandwidth and 515 nm longpass emission filter was used for the visualisation of the silica. A filter cube (Nikon G-2A) with 510–560 nm excitation bandwidth and 590 nm longpass emission filter was used for imaging the polystyrene particles. The TIFF images, acquired by the camera, were processed and analysed via custom Python code. A fluorescence intensity  $I$  vs nanoparticle concentration  $n$  calibration curve was acquired to ensure that  $I \propto n$  for any value of  $n$  examined in the experiments.

## 3. Results and discussion

### 3.1. Optimised protocol for the fabrication of microfluidic devices

The  $\Psi$ -shaped microchannels were fabricated by means of the microfluidic sticker technique [14]. A flow diagram of the process is shown in Fig. 1. Here we report the optimised fabrication protocol which was developed through experimental trial and error [31]. A SU-8 photoresist master was fabricated on a silicon wafer via standard photo-lithography technique. The CAD design of the photomask is shown in Fig. 2. The width,  $w$ , of the main channel is 400  $\mu\text{m}$ . A PDMS stamp (ca. 6 mm in thickness) was produced from the SU-8 master via replica moulding (Steps 1,2). A 250  $\mu\text{L}$  drop of NOA-81 was then sandwiched between the PDMS stamp and a flat PDMS slab (ca. 4 mm in thickness), so that the glue could spread evenly and uniformly due to the weight of the slab (Step 3). The NOA-81 layer was then exposed to UV light (ca. 365 nm) for 75 s at an intensity of 3  $\text{mW}/\text{cm}^2$  (Step 4). The exposure time was carefully chosen in order to cure the glue layer, except for the thin glue films in contact with the PDMS slab and stamp, as shown in Fig. 1. It should be noted that, since RTV 615 PDMS absorbs UV light slightly, the optimal UV exposure time depends on the thickness of the PDMS slab. Therefore, using a slab of different thickness would require to adjust the exposure time accordingly. After UV exposure, the PDMS stamp must be peeled off (Step 5), so that the partially cured and adhesive NOA layer can be glued onto another substrate. By testing the peeling step with PDMS stamps and slabs of different thicknesses –

varying within a range from 3 mm to 6 mm – it was observed that the adhesion between the NOA and PDMS layer was affected by the bending rigidity of the PDMS slab and stamp. Specifically, during peeling, the NOA-81 remains attached to the PDMS layer with the lower bending rigidity and, thus, with the smaller thickness. Consequently, to ensure that the PDMS stamp – and not the slab – is peeled off from the NOA layer, the PDMS stamp must be thicker than the PDMS slab. Once the PDMS stamp was removed, the device inlets and outlet were punched carefully on the imprinted NOA layer, laid on the PDMS slab, by means of a 1 mm diameter biopsy punch (Step 5). Punching the inlet/outlet holes on the NOA layer allows one not to drill the silicon substrates, which are fragile and can easily break. The punched NOA layer was then pressed against a silicon substrate, either flat or with microgrooves, heated to 60°C by a hot plate (Step 6). Heat prevents the formation of air bubbles upon contact between the silicon substrate and the NOA layer. Heat also promotes a weak adhesion between the silicon and the uncured NOA film, that allows one to peel of the PDMS slab. Note, that it is also possible to punch the inlet/outlet holes at this time, after the PDMS slab is removed, rather than at step 5. However, the NOA microchannel is now laying on the silicon substrate so the puncher should be handled carefully to avoid the breaking of the fragile silicon surface. For microgrooved substrates, the NOA microchannel width should be smaller than the silicon groove width to facilitate the alignment between the microchannel and the grooves. Finally, the device was exposed to UV light for 30 min at an intensity of 3  $\text{mW}/\text{cm}^2$  (Step 7) and heated to 60 °C on a hot plate for two hours to strengthen the adhesion between NOA layer and silicon substrate (Step 8). Optical micrographs of the final device are shown in Fig. 2, whereas 3D optical profiles of the microfabricated SU-8 master, the PDMS stamp and the NOA-81 channel are shown in Fig. 3. The measured depth,  $h$ , of the main channel is ca. 45  $\mu\text{m}$ .

Since cured NOA can be dissolved by chlorinated solvents, it is possible to recover the silicon substrates after device use. This feature is very important when expensive substrates, such as DRIE-fabricated silicon surfaces, are used, so that the substrates can be re-used several times and with different channel geometries. After use, the NOA-81 devices were immersed in a chloroform bath within a sealed glass container for 4–6 h to remove the cured NOA. Afterwards, the silicon substrates were recovered, rinsed with water and dried with a nitrogen stream. Fluorescent microscope observations of the silicon surfaces after treatment showed that cured NOA was effectively removed, but fluorescent silica and polystyrene nanoparticles were still contaminating the surfaces. The contaminated silicon substrates were then washed in a solution of dichloromethane (100 parts by weight), methanol (15 parts

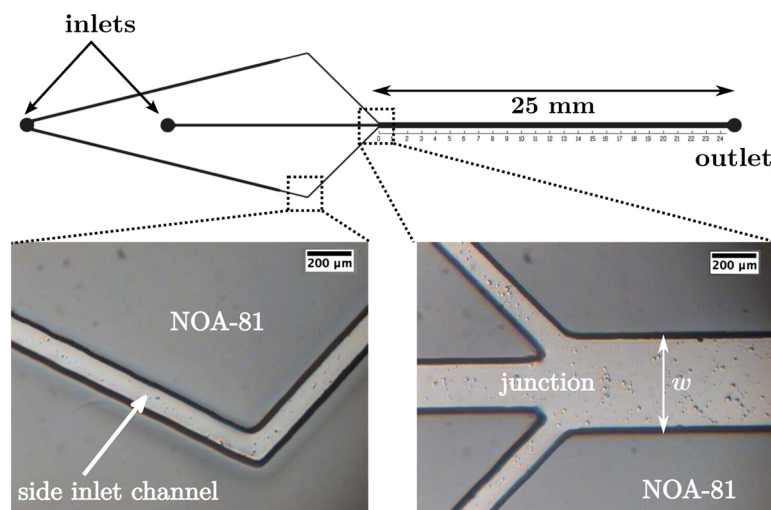
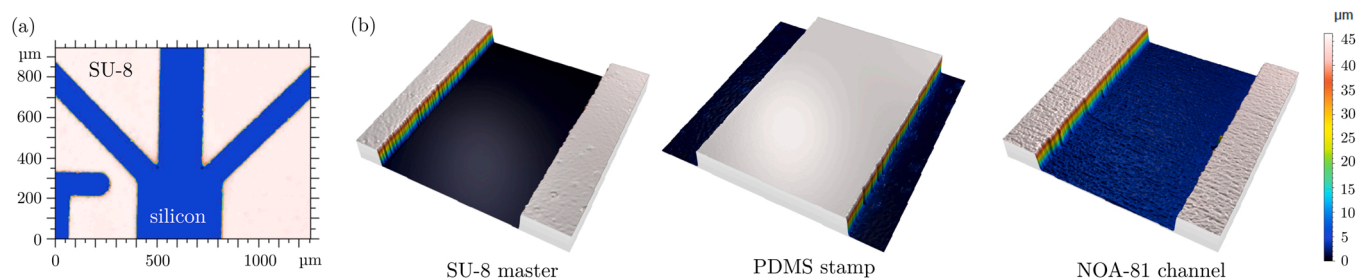


Fig. 2. CAD drawing of the photo-lithography mask, and optical micrographs of the NOA-81 microfluidic device at the side inlet channel (left) and at the junction (right). The width,  $w$ , of the main channel is 400  $\mu\text{m}$ .



**Fig. 3.** (a) Top-view of the optical profile scan of the SU-8 coated silicon master at the microchannel junction. (b) Axonometric views of the optical profile scans of the SU-8 master, PDMS stamp and NOA-81 microchannel.

by weight) and 34 % ammonium hydroxide aqueous solution (2 parts by weight) at 60 °C. Fluorescent microscope analysis confirmed the treatment efficacy in removing polystyrene nanoparticles from the silicon surfaces. Note that the same treatment is less effective for silica nanoparticles, since polystyrene can be dissolved in chlorinated solvents whereas silica can not.

### 3.2. Particle spreading and focusing on flat substrates

Steady-state salt concentration gradients were generated inside the microfluidic devices to achieve the spreading and focusing of silica and polystyrene nanoparticles by diffusiophoresis, according to a previously reported microfluidic strategy [27,29]. Previous studies adopted composite PDMS/glass flow focusing devices for generating salt concentration gradients and manipulating the particles via diffusiophoresis. This study is the first to report the use of composite NOA/silicon flow focusing devices for the spreading and focusing of nanoparticles on flat substrates. A schematic of our microfluidic set-up is shown in Fig. 4a. To generate the steady-state salt concentration gradients, parallel flows of electrolyte solutions of different ionic strengths were injected by syringe pumps into a  $\Psi$ -shaped microchannel, at equal flow rates of 12.5  $\mu\text{L}/\text{min}$ . This corresponds to an average velocity within the channel of 23.1 mm/s, calculated as the total flow rate,  $2 \times 12.5 = 25 \mu\text{L}/\text{min}$ , divided by the channel cross-section area,  $w \times h = 400 \times 45 = 2000 \mu\text{m}^2$ . The inner solution, seeded with fluorescent colloidal nanoparticles, had a lower LiCl salt concentration  $c_L = 0.1 \text{ mM}$ , and it was pumped through the central inlet of the microfluidic device. The outer flow was particle-free and it could be switched between a lower,  $c_L$ , and a higher,  $c_H = 10 \text{ mM}$  LiCl, salt solution by means of a flow switching valve. Fig. 4b shows the schematic of the microdevice, fitted with a flat silicon substrate, together with the imaging acquisition system adopted to investigate the dynamics of

fluorescent colloidal particles in the microchannels.

The distribution of silica nanoparticles in the microchannel with and without a salt concentration gradient, is shown in Fig. 5. The outer stream consisted of a 1 mM TRIS buffer (pH = 9) and low ( $c_L$ ) salt solution seeded with silica nanoparticles at a concentration of  $n_0 = 0.005 \%$  v/v. TRIS buffer has a dissociation constant of approximately 8.1 at 25 °C and it is an effective buffer in the range of pH 7–9 [32]. Thus, TRIS buffer allows to stabilise the surface charge of silica particles and maintains the particle zeta potential to the desired value [27]. The outer stream was also a 1 mM TRIS buffer (pH = 9) solution, but its salt concentration was varied over time between  $c_L$  and  $c_H$ , as shown in Fig. 5c. The time evolution of the fluorescent colloid distribution within the channel is shown by the epi-fluorescence micrographs in Fig. 5d. The micrographs were acquired at a distance of 10 mm from the junction, i.e. at  $z/w = 25$ , where  $z$  is the longitudinal distance from the channel junction. In Fig. 5,  $t = 0$  is an arbitrarily chosen time after flow stabilisation. By imposing a salt concentration gradient at time  $t > 5 \text{ min}$ , the colloidal particles spread spontaneously from the centre towards the outer regions of the channel and accumulated at two symmetric focusing regions at the edges of the colloid flow stream, namely  $x/w \simeq \pm 0.25$ , where  $x$  is the transverse distance from the centre of the channel. The width,  $w_c(t)$ , of the fluorescent colloidal stream increased from 200  $\mu\text{m}$  to 240  $\mu\text{m}$ . The homogeneous particle distribution within the central region of the channel was recovered when the salt concentration gradient was removed ( $t > 15 \text{ min}$ ). The time evolution of the fluorescence intensity profiles along the channel transverse direction,  $x$ , is shown in Fig. 5e. The fluorescence intensity  $I$ , which is proportional to the particle concentration  $n$ , is normalised with respect to the fluorescence intensity  $I_0$  of the colloidal solution injected in the inner channel of the device. The transverse distance  $x$  is also normalised with respect to the channel width  $w$ . The fluorescence intensity profile in presence of salt concentration gradient (red curve) was wider than the one in

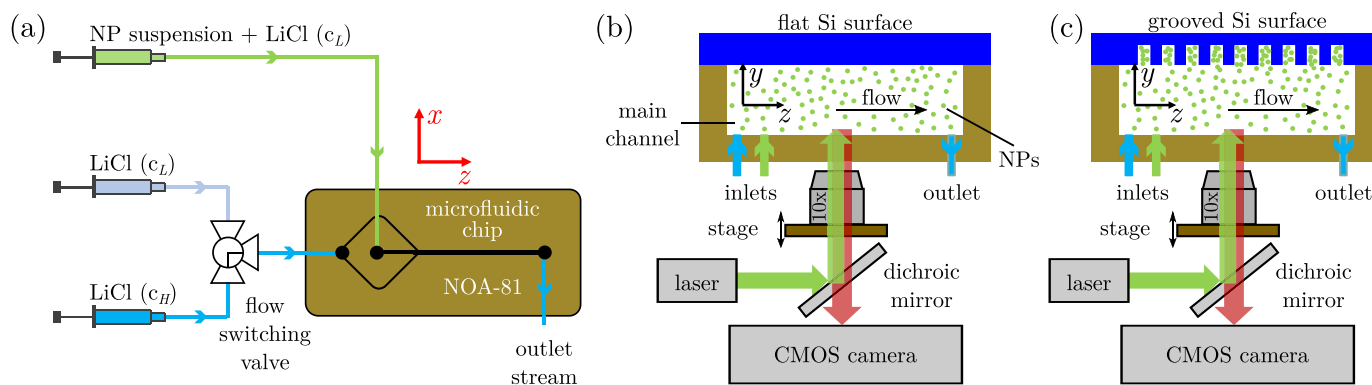


**Fig. 4.** (a) Schematic of the microfluidic set-up. A flow switching valve was used to create a steady-state salt concentration gradient in the flow focusing  $\Psi$ -junction device by switching the side streams between LiCl solutions at low ( $c_L$ ) and high ( $c_H$ ) concentration. The central stream consisted of nanoparticle (NP) suspension at low salt concentration. (b-c) Schematics of the epifluorescence microscope rig used for the visualisation of the particle distribution in the microfluidic devices fitted with either a flat or microgrooved silicon (Si) surface.

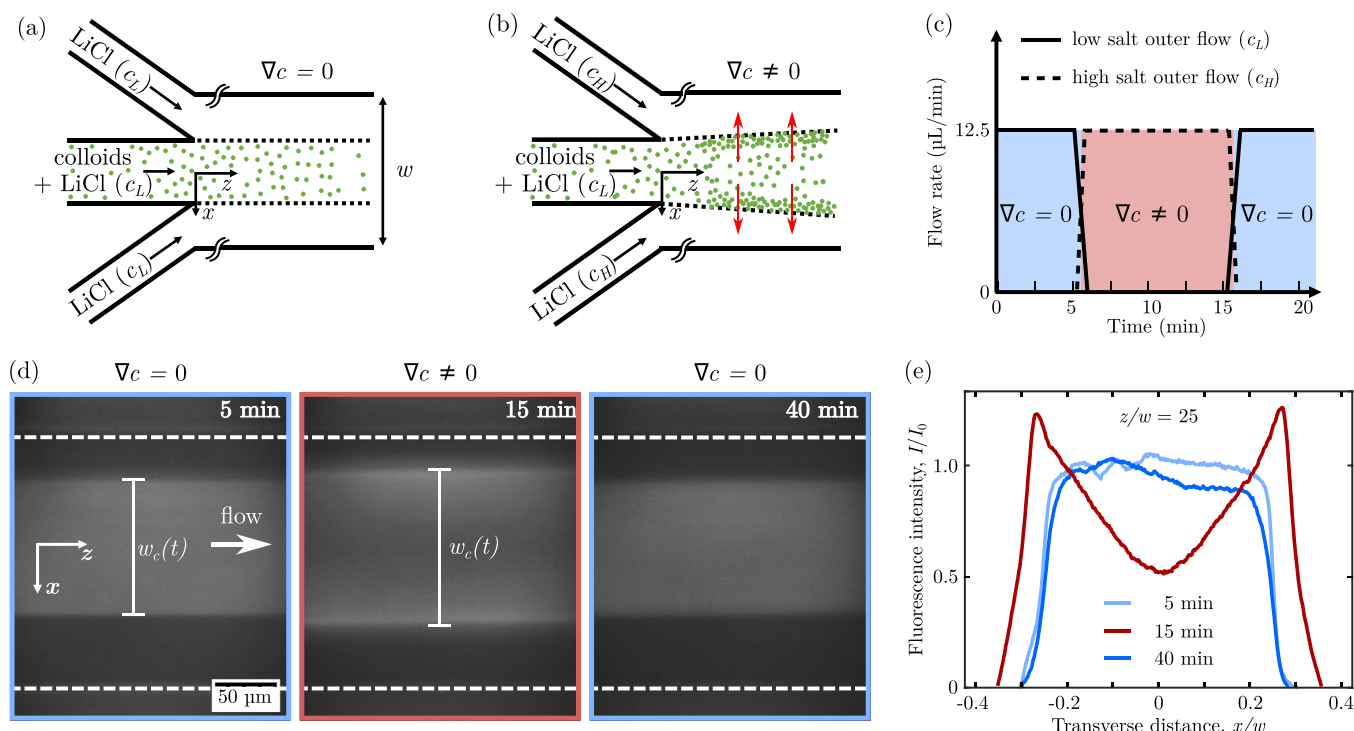


**Fig. 5.** Diffusiophoresis-driven focusing of 200 nm diameter silica particles (0.005 % v/v) in a NOA-81  $\Psi$ -junction device with a flat silicon surface. (a-b) Flow configuration in the  $\Psi$ -junction device in absence (a) and presence (b) of a steady salt concentration gradient. (c) Time-evolution of the flow rates of the low and high salt outer streams, achieved via the flow switching valve. The red (blue) shaded regions correspond to the presence (absence) of the steady salt concentration gradient,  $\nabla c$ . (d) Epi-fluorescence micrographs of the main channel at 10 mm ( $z/w = 25$ ) downstream of the junction, before ( $t = 5$  min), during ( $t = 15$  min) and after ( $t = 40$  min) imposing the steady salt concentration gradient. The white dashed lines represent the channel boundaries, and the solid lines indicate the width,  $w_c(t)$ , of the fluorescent colloidal stream. (e) Normalised fluorescence intensity profiles along the transverse direction, corresponding to the micrographs in panel (d).

absence of a salt concentration gradient (blue curves), because of the diffusiophoresis velocity,  $v_{DP} = \Gamma_{DP} \nabla c / c$ , that drives the nanoparticles from the inner low salt concentration region to the outer high salt concentration regions - with  $\Gamma_{DP} > 0$  being the diffusiophoresis coefficient. The non-linear scaling  $v_{DP} \propto \nabla c / c$  results in a diffusiophoresis velocity  $v_{DP}$  decreasing from the centre (low salt) towards the outer (high salt) regions of the channel [27]. Consequently, two symmetric particle focusing peaks appeared at the interface between the inner and outer streams, while the colloid concentration in the central region of the channel decreased. These observations are in agreement with those reported by Abecassis et al. [27,28], who investigated the spreading and

focusing of 200 nm silica particles under the same flow conditions, but in composite PDMS/glass flow focusing junction devices. Interestingly, in these previous studies no diffusiophoresis flow [25], dragging colloids from high to low salt regions, could be observed, despite PDMS being negatively charged [33]. Since our devices were made of hydrophilic (silicon and NOA-81) rather than hydrophobic (PDMS) materials, it can be expected that the channel walls of our devices bear a higher surface charge compared to PDMS channels used in previous studies. This could lead to the onset of a diffusiophoresis flow with a wall slip velocity,  $v_{DO} = -\Gamma_{DO} \nabla c / c$ , with  $\Gamma_{DO}$  the diffusiophoresis coefficient. However, under the examined experimental conditions, no diffusiophoresis flows

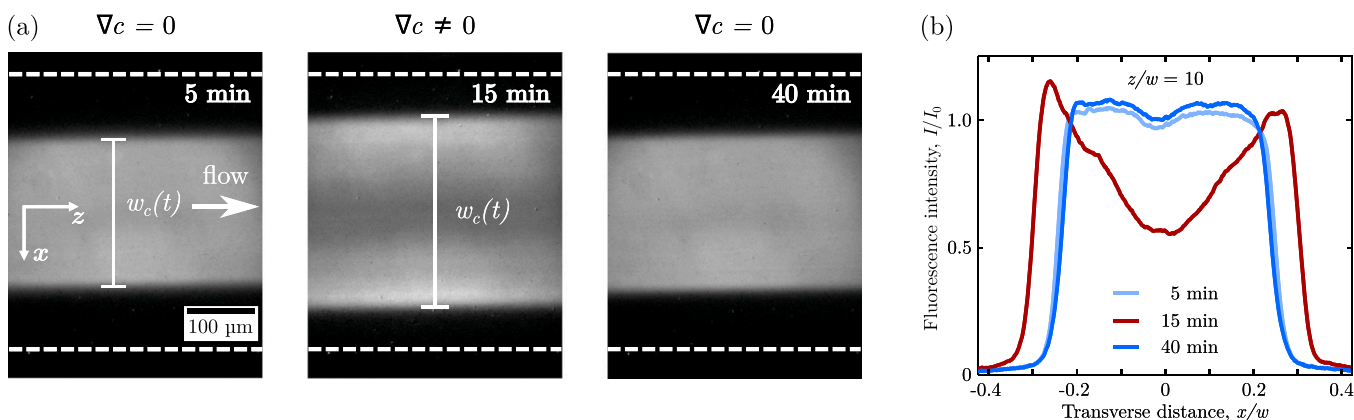


**Fig. 6.** Diffusiophoresis-driven focusing of 200 nm diameter polystyrene particles (0.005 % v/v) in a NOA-81  $\Psi$ -junction device with a flat silicon surface. (a) Epi-fluorescence micrographs of the main channel at 4 mm ( $z/w = 10$ ) downstream of the junction, before ( $t = 5$  min), during ( $t = 15$  min) and after ( $t = 40$  min) imposing the steady salt concentration gradient. The white dashed lines represent the channel boundaries. (b) Normalised fluorescence intensity profiles along the transverse direction, corresponding to the micrographs in panel (a). The red (blue) curve corresponds to the presence (absence) of the steady salt concentration gradient,  $\nabla c$ .

dragging particles from high to low salt regions could be seen. Note that this does not imply necessarily that there are no diffusioosmosis flows in the system, but just that they are not intense enough to overcome the particle diffusio-phoresis migration from low to high salt regions. Finally, upon removal of the salt concentration gradient, the diffusio-phoresis migration of particles ceased and the width of the colloidal intensity profiles,  $w_c(t)$ , reverted to its original size (Fig. 5d,e).

Similar experiments were repeated with polystyrene nanoparticles and the results are shown in Fig. 6. The inner stream consisted of a DI water suspension of polystyrene nanoparticles at low  $c_L$  salt concentration, whereas the outer stream was a DI water solution with a salt concentration varied over time between  $c_L$  and  $c_H$ . The time evolution of the colloid distribution in a flat silicon device is also shown in Fig. 6. At a distance of 4 mm from the junction (i.e.  $z/w = 10$ ), the width  $w_c(t)$  of the fluorescent colloidal stream increased from 200  $\mu\text{m}$  to 250  $\mu\text{m}$  upon imposition of the steady salt concentration gradient. Compared to the silica nanoparticle experiments, the larger expansion of the colloidal stream at a closer distance from the junction can be explained by the more negative zeta potential of polystyrene nanoparticles ( $\zeta = -58.5 \pm 1$  mV) compared to the one of silica nanoparticles ( $\zeta = -41.7 \pm 4$  mV). This results in a higher diffusio-phoresis coefficient  $\Gamma_{DP}$ , and thus a larger diffusio-phoresis velocity,  $v_{DP}$ , which led to a wider particle spreading. It can be concluded that, for a given salt concentration gradient, a higher surface charge of the nanoparticles results in a wider particle spreading over flat silicon substrates. Potentially, such a behaviour could be exploited for the characterisation of nanoparticle zeta potential by relating the latter with particle spreading via a calibration procedure.

### 3.3. Particle accumulation in microgrooved substrates

In these experiments, NOA-81 devices fitted with a microgrooved

surface were used, as shown schematically in Fig. 4c. In a previous study [29], we introduced a microfluidic strategy for the rapid and steady accumulation of nanoparticles within the 8  $\mu\text{m}$  thick grooves of a microstructured silicon surface. Here, we adopted the same strategy, but microstructured silicon surfaces with 24  $\mu\text{m}$  thick grooves were used instead. The results for silica nanoparticles are reported in Fig. 7. The inner and outer streams are identical to those used in the experiments with the flat substrate devices. However, to improve the signal-to-noise ratio of the epi-fluorescence micrographs, the initial concentration of silica nanoparticles in the inner stream,  $n_0$ , was increased to 0.05 % v/v. The time evolution of the outer stream flow rates is shown in Fig. 7c. As in previous experiments,  $t = 0$  is an arbitrarily chosen time after flow stabilisation, but before the imposition of the salt concentration gradient. Fig. 7d shows the epi-fluorescence micrographs of the device at 10 mm downstream of the junction ( $z/w = 25$ ) under varying flow arrangements for salt solutions. The micrographs were acquired with the focal plan of the microscope objective located at the entrance of the surface grooves, as shown in the inset of Fig. 7d. The depth of field of the microscope (namely, the thickness of the slice region that is in acceptably sharp focus in the micrographs) can be estimated [34] as  $d = n_{ref} \lambda_{em}/NA^2 + n_{ref} e/(M \cdot NA) \simeq 10 \mu\text{m}$ , where  $n_{ref} = 1$  is the refractive index of the objective immersion medium (air),  $\lambda_{em} = 510$  nm is the nanoparticle emission wavelength,  $e = 4.8 \mu\text{m}$  is the pixel pitch of the CMOS camera,  $NA = 0.25$  and  $M = 10$  are the objective numerical aperture and magnification, respectively. As a result, the micrographs captured the fluorescence intensity of nanoparticles located either in the main channel or inside the microgrooves, at few microns from the groove entrance. As expected, in absence of a salt concentration gradient ( $t < 15$  min), the colloids remained evenly distributed in the central region of the channel (Fig. 7d). Upon injection of the higher salt outer stream ( $t > 15$  min), a steady salt concentration gradient was generated in the transverse direction (red arrows in Fig. 7b), leading to colloid

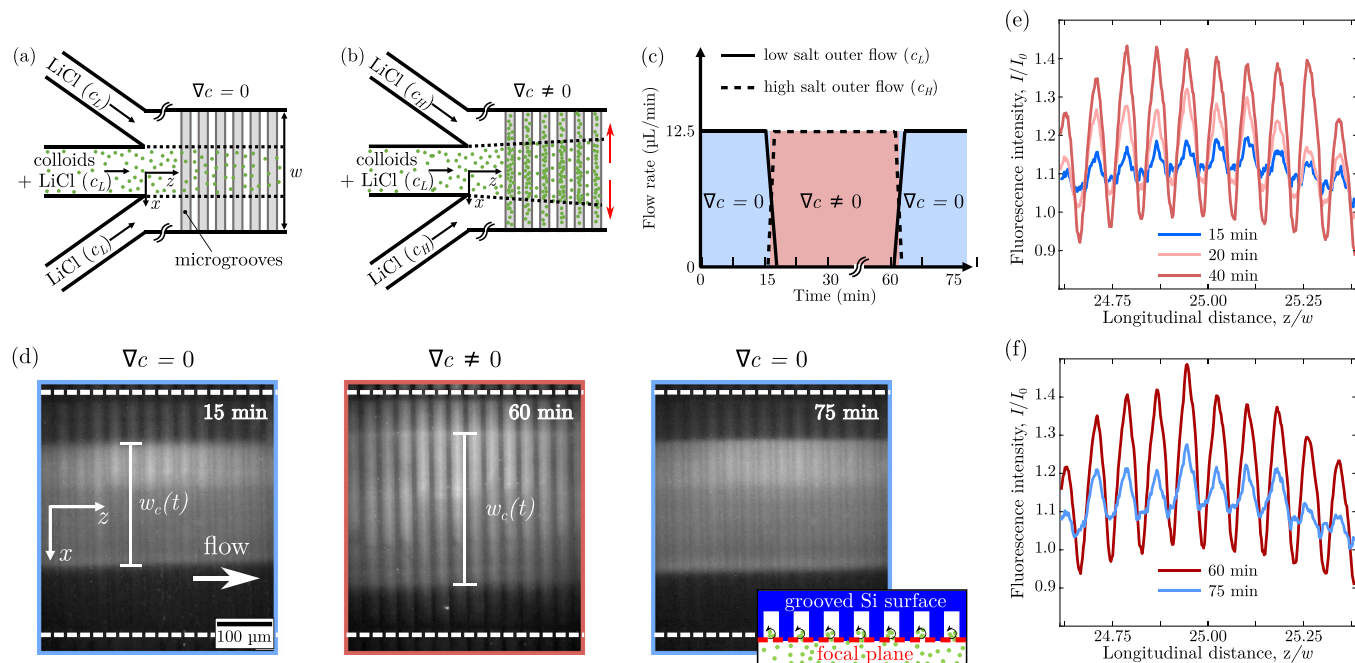


**Fig. 7.** Diffusiophoresis-driven accumulation of 200 nm diameter silica particles (0.05 % v/v) in the microgrooves of a NOA-81  $\Psi$ -junction device. (a-b) Flow configuration in the  $\Psi$ -junction device in absence (a) and presence (b) of a steady salt concentration gradient. Red arrows show the direction of the salt concentration gradient. The grey-shaded regions corresponds to the microgrooves in the silicon substrate. (c) Time-evolution of the flow rates of the low and high salt outer streams, achieved via the flow switching valve. The red (blue) shaded regions correspond to the presence (absence) of the steady salt concentration gradient,  $\nabla c$ . (d) Epi-fluorescence micrographs of the main channel at 10 mm ( $z/w = 25$ ) downstream of the junction, before ( $t = 15$  min), during ( $t = 60$  min) and after ( $t = 75$  min) imposing the steady salt concentration gradient. The white dashed lines represent the channel boundaries. (e-f) Time evolution of the normalised fluorescence intensity profiles along the longitudinal direction. The profiles are calculated by averaging the intensity along the transverse direction. Red (blue) curves correspond to the presence (absence) of the salt concentration gradient.

spreading along the same direction (i.e. wider  $w_c$ ) as it occurred in the case of the flat silicon substrate. As previously reported [29], a component of the salt concentration gradient along the channel depth direction is originated by the Poiseuille-like velocity profile in the rectangular channel. This component leads to the diffusiophoresis migration of colloids from the channel bulk into the grooves, as confirmed by the micrograph at  $t = 60$  min showing brighter transverse regions corresponding to the locations of the surface microgrooves. Differently from what was previously observed in  $T = 8 \mu\text{m}$  thick microgrooves, for the examined surface ( $T = 24 \mu\text{m}$ ) the colloids were homogeneously distributed inside the grooves along the transverse ( $x$ ) direction. More interestingly, the colloids inside the grooves migrated towards the outer stream regions and spread well beyond the width,  $w_c(t)$ , of the fluorescent colloidal stream. Our previous study [29] demonstrated that particle accumulation results from the combined effects of diffusiophoresis transport and hydrodynamic flow recirculation within the grooves. Thus, it can be expected that a change in groove thickness affects the flow field within the grooves and, consequently, the particle distribution therein. As the outer stream was switched back to the lower salt solution, the effect of particle accumulation within the grooves disappeared and the initial particle distribution within the channel was recovered ( $t = 75$  min). Fig. 7e-f show the time evolution of the normalised fluorescence intensity profile along the flow (longitudinal) direction,  $z$ . It can be observed that without salt concentration gradient (blue curve), the intensity profile had an oscillating trend with a wavelength matching the groove pitch,  $L = 24 \mu\text{m}$ . It is hypothesised that, in the absence of a salt concentration gradient, particles could enter the groove by advection along the flow streamlines that formed a recirculation region at the groove entrance – see inset in Fig. 7d. However, particles could not travel further down the grooves due to their low diffusivity. As a result, there is a correlation between the peaks of the fluorescence intensity profile and the groove locations. For  $t > 15$  min, the salt concentration gradient caused the accumulation of particles within the grooves, as demonstrated by the higher peaks in the corresponding intensity profiles (red curves). A steady-state distribution of particles within the grooves was achieved ca. 20 min after the outer flow was switched and the salt concentration gradient was imposed. Particles could diffuse out of the grooves once the salt concentration gradient was removed, as confirmed by the intensity profile at  $t = 75$  min. These results demonstrated that the particle trapping and accumulation phenomenon is fully reversible.

Similar experiments were repeated with the polystyrene nanoparticles and the corresponding results are showed in Fig. 8. Again, the inner and outer streams were identical to those used in the experiments

with the flat substrate devices, but the initial concentration of particles in the inner stream,  $n_0$ , was increased to 0.05 % v/v. As it can be expected, the higher diffusiophoresis coefficient of polystyrene colloids resulted in a more intense accumulation of nanoparticles within the grooves of the structured silicon surface, as shown by the fluorescence micrographs and intensity profiles in Fig. 8. Consequently, also this particle manipulation strategy could be exploited potentially for the characterisation of colloid zeta potential, once the intensity of the focusing peak is correlated to the particle zeta potential via calibration.

### 3.4. Synthesis of liposomes

In this last set of experiments, NOA flow focusing devices fitted with a flat silicon substrate were used to generate chemical concentration gradients between an aqueous and alcohol phase to synthesise nanoscale lipid vesicles according to the hydrodynamic focusing procedure introduced by Jahn et al. [21]. The synthesis of liposomes by hydrodynamic focusing has been previously reported in glass capillaries [35,36] as well as PDMS [37,38] and glass [39] flow focusing junction devices. This approach has also been adopted for the concurrent loading of hydrophilic or hydrophobic drugs, dispersed either in the aqueous or alcohol phase, respectively [40]. It is worth noting that the excellent chemical resistance of glass devices allows for a wider selection of solvents that can be used for the lipid and hydrophobic drug solutions, compared to PDMS devices. However, the manufacturing of glass flow focusing devices is more complicated and expensive than PDMS chips. NOA flow focusing devices, instead, combine good chemical resistance with easy and cost-effective fabrication procedures. To date, to best of our knowledge, only one study [24] demonstrated the formation of liposomes using a composite NOA/polystyrene flow focusing device. However, the device geometry was rather complex, including seven converging inlet channels and an array of staggered herringbones on the side of the main channels to promote micromixing. In this study, we demonstrate that a composite NOA/silicon flow focusing device with a plain  $\Psi$ -junction geometry is sufficient to produce liposome population with a controlled narrow size distribution.

In these experiments, the outer streams consisted of a buffer aqueous solution, containing 5  $\mu\text{M}$  EDTA, 5  $\mu\text{M}$  HEPES and 0.01 mM LiCl, whereas the inner stream was an ethanol solution with DOPC lipids at a concentration of 15 mg/mL. A schematic of the flow configuration is shown in Fig. 9a. Under these conditions, ethanol and lipid molecules diffuse into the buffer solution while the water molecules diffuse into the alcohol phase. As the solubility limit of the lipids is exceeded, they self-assemble into disk-like bilayered lipid fragments. These flat lipid

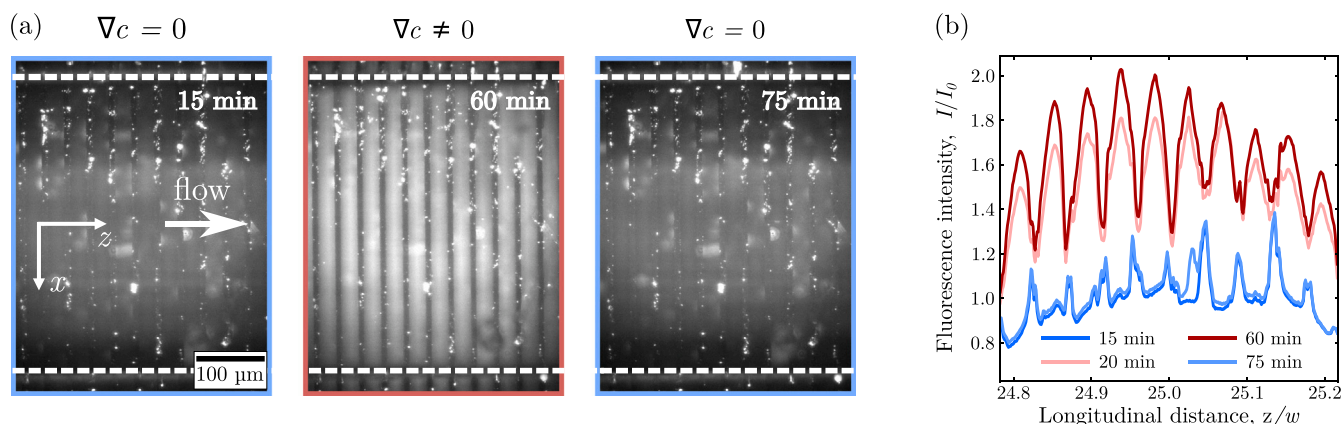


**Fig. 8.** Diffusiophoresis-driven accumulation of 200 nm diameter polystyrene particles (0.05 % v/v) in the microgrooves of a NOA-81  $\Psi$ -junction device. (a) Epifluorescence micrographs of the main channel at 10 mm ( $z/w = 25$ ) downstream of the junction, before ( $t = 15$  min), during ( $t = 60$  min) and after ( $t = 75$  min) imposing the steady salt concentration gradient. The white dashed lines represent the channel boundaries. (b) Time evolution of the normalised fluorescence intensity profiles along the longitudinal direction. The profiles are calculated by averaging the intensity along the transverse direction. Red (blue) curves correspond to the presence (absence) of the steady salt concentration gradient,  $\nabla c$ .



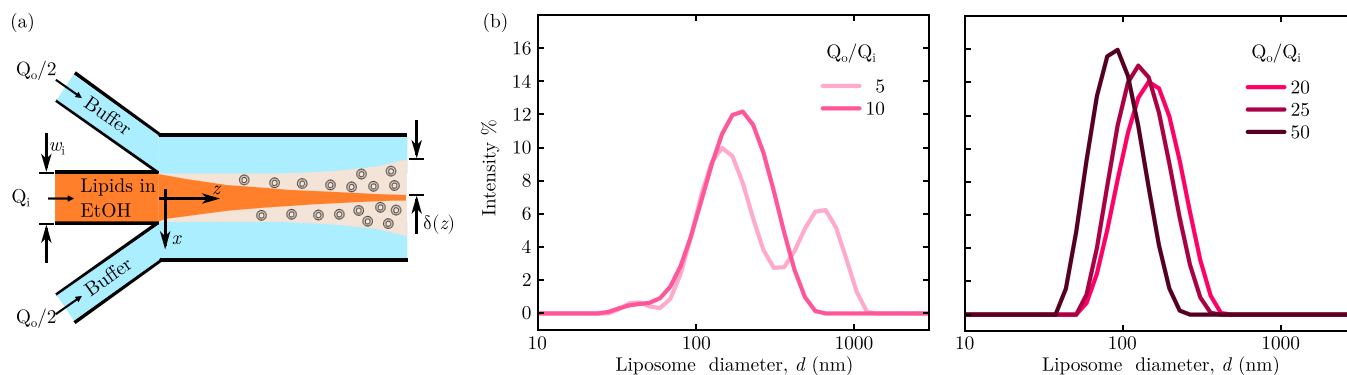


**Fig. 9.** Synthesis of DOPC liposomes by hydrodynamic focusing. (a) Schematic of the NOA  $\Psi$ -junction device fitted with a flat silicon substrate. The inner lipid-ethanol stream, with a flow rate  $Q_i$ , is hydrodynamically focused by the outer buffer stream, with a flow rate  $Q_o$ . (b) Size distribution of liposomes generated under varying flow rate ratios,  $Q_o/Q_i$ . The Z-average particle sizes,  $\bar{d}$ , and polydispersity index, PDI, are i)  $Q_o/Q_i = 5$ ,  $\bar{d} = 259 \pm 11$  nm,  $PDI = 0.462$  ii)  $Q_o/Q_i = 10$ ,  $\bar{d} = 160 \pm 3$  nm,  $PDI = 0.182$  iii)  $Q_o/Q_i = 20$ ,  $\bar{d} = 141 \pm 4$  nm,  $PDI = 0.082$  iv)  $Q_o/Q_i = 25$ ,  $\bar{d} = 127 \pm 1$  nm,  $PDI = 0.176$  v)  $Q_o/Q_i = 50$ ,  $\bar{d} = 88 \pm 2$  nm,  $PDI = 0.144$ .

structures grow and bend until they form stable closed vesicles at the interface between the two phases [41,42]. In our experiments, the flow rate of the outer stream,  $Q_o$ , was kept at 50  $\mu\text{L}/\text{min}$ , and the ratio between the outer and inner flow rates,  $Q_o/Q_i$ , was varied between 5 and 50. The corresponding average flow velocities,  $U_{av}$ , varied between 56 mm/s and 47 mm/s. It is worth noting that full mixing between phases occurs when the thickness of the interfacial diffusion layer between the two phases,  $\delta(z)$ , matches half the width of the inner channel  $w_i = 100$   $\mu\text{m}$  (Fig. 9a). In the bulk of the rectangular microchannel, namely away from the top and bottom walls, the function  $\delta(z)$  can be approximated as  $\delta(z) \simeq \sqrt{D_{eth} z / U_{av}}$ , where  $D_{eth} = 0.89 \times 10^{-9}$   $\text{m}^2/\text{s}$  is the diffusion coefficient of ethanol in water [43]. Conversely, near the top and bottom walls of the device,  $\delta(z) \simeq (D_{eth} zh / U_{av})^{1/3}$ , due to the Poiseuille-like velocity profile along the channel depth direction [44]. It follows that at the outlet of the device ( $z = 25$  mm), the thickness of the diffusion layer is 21  $\mu\text{m}$  and 28  $\mu\text{m}$  in the bulk and near the walls, respectively. This is only 20 % of inner channel width, hence full mixing is not achieved in the device.

The resulting liposome distribution for varying flow rate ratios are reported in Fig. 9b. At low flow rate ratios and, thus, low shear forces, liposomes can aggregate into clusters and bilayer defects may induce the fusion of adjacent liposomes [45]. This mechanism could explain the observation of two peaks in the particle size distribution at the lowest flow ratio  $Q_o/Q_i = 5$ . At higher flow rate ratios, a single population of particle size distribution can be achieved, suggesting that liposome aggregation and fusion are no longer occurring under these shear stress conditions. It can also be observed that the average liposome size decreases with increasing flow rate ratios, in agreement with previous studies [41,45,46]. To conclude, composite NOA/silicon flow junction devices can be used successfully to generate liposome population with a narrow size distribution that can be controlled by adjusting the ratio between the flow rates of the buffer and alcohol streams.

#### 4. Conclusions

NOA microfluidic devices, manufactured via microfluidic sticker technique, provide an effective alternative option to PDMS devices due to their many advantages, including improved optical transparency, chemical resistance to many organic solvents, gas impermeability, and high mechanical stiffness. In this study, we reported the optimised protocol for the fabrication of composite NOA/silicon devices with a flow focusing junction. The devices fitted with flat silicon substrates were used to generate steady-state salt concentration gradients to achieve the spreading and focusing of silica and polystyrene nanoparticles. Wider spreading toward the high salt concentration regions was observed for the particles (polystyrene) with a more negative zeta

potential. Despite the hydrophilic NOA and silicon walls of the channels bear a negative surface charge, diffusioosmosis flows dragging the colloids from high to low salt regions could not be detected, hence confirming that particle diffusiophoresis is the main mechanism governing the particle dynamics. These observations are in agreement with previously reported particle spreading experiments in composite hydrophobic PDMS/hydrophilic glass devices [27]. We also demonstrated the accumulation of silica and polystyrene particles within the grooves of NOA flow focusing devices fitted with silicon microgrooved substrates. In a previous study, we showed that, for 8  $\mu\text{m}$  thick grooves, particles accumulated at the centre of the channel, while here we demonstrated that, for 24  $\mu\text{m}$  thick grooves, particles are evenly accumulated within the groove along the whole channel width. This is probably due to the fact that the groove thickness affects the hydrodynamic flow field, which in turn determines the particle distribution within the grooves. Furthermore, our experimental observations led us to conclude that particles (polystyrene) with a more negative zeta potential tends to get more concentrated within the device grooves, thereby suggesting a potential strategy for the characterisation of particle zeta potential based on the fluorescence intensity of the accumulation peaks within the grooves. Finally, we showed that composite NOA/silicon flow focusing devices with a  $\Psi$ -junction can be successfully used for the synthesis of DOPC liposomes with a narrow size distribution controlled by the flow rate ratio between the hydrodynamically focused streams. Compared with existing NOA microdevices for liposome synthesis, our flow focusing chip has a much simpler geometry, which facilitates the device fabrication and operation procedures. In conclusions, this study showcases the potential of NOA flow focusing devices for the synthesis and manipulation of nanoparticles, which could underpin a variety of microfluidic applications, such as drug synthesis and encapsulation, bioanalysis, nanoparticle characterisation and filtration.

#### CRediT authorship contribution statement

**Naval Singh:** Methodology, Investigation, Formal analysis, Funding acquisition, Writing - original draft, Writing - review & editing. **Adnan Chakra:** Methodology, Investigation, Writing - original draft, Writing - review & editing. **Goran T. Vladislavljević:** Conceptualization, Methodology, Supervision, Writing - review & editing. **Cécile Cottin-Bizonne:** Methodology, Supervision, Writing - review & editing. **Christophe Pirat:** Methodology, Supervision, Writing - review & editing. **Guido Bolognesi:** Conceptualization, Methodology, Supervision, Funding acquisition, Writing - original draft, Writing - review & editing.

## Declaration of Competing Interest

The authors declare that they have no known competing financial interests or personal relationships that could have appeared to influence the work reported in this paper.

## Data availability

The authors confirm that the data supporting the findings of this study are available within the article.

## Acknowledgements

This research was supported by the EPSRC (EP/S013865/1) and the Santander Mobility Grant awarded to NS.

## References

- B.K. Gale, A.R. Jafek, C.J. Lambert, B.L. Goenner, H. Moghimifam, U.C. Nze, S. K. Kamarapu, A review of current methods in microfluidic device fabrication and future commercialization prospects, *Inventions* 3 (3) (2018) 60.
- A. Manz, D.J. Harrison, E.M. Verpoorte, J.C. Fettinger, A. Paulus, H. Lüdi, H. M. Widmer, Planar chips technology for miniaturization and integration of separation techniques into monitoring systems: capillary electrophoresis on a chip, *J. Chromatogr. A* 593 (1–2) (1992) 253–258.
- D.R. Reyes, D. Iossifidis, P.-A. Auroux, A. Manz, Micro total analysis systems. 1. introduction, theory, and technology, *Anal. Chem.* 74 (12) (2002) 2623–2636.
- G.M. Whitesides, The origins and the future of microfluidics, *Nature* 442 (7101) (2006) 368–373.
- S.D. Senturia, *Microsystem Design*, Springer Science & Business Media, 2007.
- C. Iliescu, H. Taylor, M. Avram, J. Miao, S. Franssila, A practical guide for the fabrication of microfluidic devices using glass and silicon, *Biomicrofluidics* 6 (1) (2012), 016505.
- R.Al Nuamani, G. Bolognesi, G.T. Vladislavjević, Microfluidic production of poly (1, 6-hexanediol diacrylate)-based polymer microspheres and bifunctional microcapsules with embedded TiO<sub>2</sub> nanoparticles, *Langmuir* 34 (39) (2018) 11822–11831.
- R.Al Nuamani, S.K. Smoukov, G. Bolognesi, G.T. Vladislavjević, Highly porous magnetic janus microparticles with asymmetric surface topology, *Langmuir* 36 (42) (2020) 12702–12711.
- T. Deydier, G. Bolognesi, G.T. Vladislavjević, Scaled-up droplet generation in parallelised 3d flow focusing junctions, *Colloids Surf. A: Physicochem. Eng. Asp.* 641 (2022), 128439.
- P.N. Nge, C.I. Rogers, A.T. Woolley, Advances in microfluidic materials, functions, integration, and applications, *Chem. Rev.* 113 (4) (2013) 2550–2583.
- C.-W. Tsoo, Polymer microfluidics: Simple, low-cost fabrication process bridging academic lab research to commercialized production, *Micromachines* 7 (12) (2016) 225.
- J.C. McDonald, D.C. Duffy, J.R. Anderson, D.T. Chiu, H. Wu, O.J. Schueller, G. M. Whitesides, Fabrication of microfluidic systems in poly (dimethylsiloxane), *Electrophor.: Int. J.* 21 (1) (2000) 27–40.
- J.C. McDonald, G.M. Whitesides, Poly (dimethylsiloxane) as a material for fabricating microfluidic devices, *Acc. Chem. Res.* 35 (7) (2002) 491–499.
- D. Bartolo, G. Degré, P. Nghe, V. Studer, Microfluidic stickers, *Lab Chip* 8 (2) (2008) 274–279.
- T. Fu, Y. Wu, Y. Ma, H.Z. Li, Droplet formation and breakup dynamics in microfluidic flow-focusing devices: from dripping to jetting, *Chem. Eng. Sci.* 84 (2012) 207–217.
- L. Martín-Banderas, M. Flores-Mosquera, P. Riesco-Chueca, A. Rodríguez-Gil, Á. Cebolla, S. Chávez, A.M. Gañán-Calvo, Flow focusing: a versatile technology to produce size-controlled and specific-morphology microparticles, *Small* 1 (7) (2005) 688–692.
- S.-Y. Teh, R. Lin, L.-H. Hung, A.P. Lee, Droplet microfluidics, *Lab Chip* 8 (2) (2008) 198–220.
- G. Bolognesi, A. Hargreaves, A.D. Ward, A.K. Kirby, C.D. Bain, O. Ces, Microfluidic generation of monodisperse ultra-low interfacial tension oil droplets in water, *RSC Adv.* 5 (11) (2015) 8114–8121.
- M. Lu, A. Ozcelik, C.L. Grigsby, Y. Zhao, F. Guo, K.W. Leong, T.J. Huang, Microfluidic hydrodynamic focusing for synthesis of nanomaterials, *Nano Today* 11 (6) (2016) 778–792.
- M. Rhee, P.M. Valencia, M.I. Rodriguez, R. Langer, O.C. Farokhzad, R. Karnik, Synthesis of size-tunable polymeric nanoparticles enabled by 3d hydrodynamic flow focusing in single-layer microchannels, *Adv. Mater.* 23 (12) (2011) H79–H83.
- A. Jahn, W.N. Vreeland, M. Gaitan, L.E. Locascio, Controlled vesicle self-assembly in microfluidic channels with hydrodynamic focusing, *J. Am. Chem. Soc.* 126 (9) (2004) 2674–2675.
- A. Zizzari, L. Carbone, M. Cesaria, M. Bianco, E. Perrone, F. Rendina, V. Arima, Continuous flow scalable production of injectable size-monodisperse nanoliposomes in easy-fabrication milli-fluidic reactors, *Chem. Eng. Sci.* 235 (2021), 116481.
- H. Aghaei, A.R. Solaimany Nazar, Continuous production of the nanoscale liposome in a double flow-focusing microfluidic device, *Ind. Eng. Chem. Res.* 58 (51) (2019) 23032–23045.
- D. Witzigmann, S. Sieber, F. Porta, P. Grossen, A. Bieri, N. Strelnikova, T. Pfohl, C. Prescianotto-Baschong, J. Huwyler, Formation of lipid and polymer based gold nano-hybrids using a nanoreactor approach, *RSC Adv.* 5 (91) (2015) 74320–74328.
- J.L. Anderson, Colloid transport by interfacial forces, *Annu. Rev. Fluid Mech.* 21 (1) (1989) 61–99.
- S. Shin, Diffusiophoretic separation of colloids in microfluidic flows, *Phys. Fluids* 32 (10) (2020), 101302.
- B. Abécassis, C. Cottin-Bizonne, C. Ybert, A. Ajdari, L. Bocquet, Boosting migration of large particles by solute contrasts, *Nat. Mater.* 7 (10) (2008) 785–789.
- B. Abécassis, C. Cottin-Bizonne, C. Ybert, A. Ajdari, L. Bocquet, Osmotic manipulation of particles for microfluidic applications, *N. J. Phys.* 11 (7) (2009), 075022.
- N. Singh, G.T. Vladislavjević, F. Nadal, C. Cottin-Bizonne, C. Pirat, G. Bolognesi, Reversible trapping of colloids in microgrooved channels via diffusiophoresis under steady-state solute gradients, *Phys. Rev. Lett.* 125 (24) (2020), 248002.
- R.J. Hunter, *Foundations of Colloid Science*, Oxford University Press, 2001.
- N. Singh, *Manipulation of colloidal particles by solute gradients in continuous-flow microfluidic devices*, Ph.D. thesis, Loughborough University (2021). (<https://rpository.lboro.ac.uk/account/articles/14891400>).
- A. Sikora, D. Bartczak, D. Geißler, V. Kestens, G. Roebben, Y. Ramaye, Z. Varga, M. Palmi, A.G. Shard, H. Goenaga-Infante, et al., A systematic comparison of different techniques to determine the zeta potential of silica nanoparticles in biological medium, *Anal. Methods* 7 (23) (2015) 9835–9843.
- B.J. Kirby, E.F. Hasselbrink Jr, Zeta potential of microfluidic substrates: 2. data for polymers, *Electrophoresis* 25 (2) (2004) 203–213.
- B.E. Saleh, M.C. Teich, *Fundamentals of Photonics*, John Wiley & Sons, 2019.
- G.T. Vladislavjević, A. Laouini, C. Charcosset, H. Fessi, H.C. Bandulasena, R. G. Holdich, Production of liposomes using microengineered membrane and co-flow microfluidic device, *Colloids Surf. A: Physicochem. Eng. Asp.* 458 (2014) 168–177.
- R. Othman, G.T. Vladislavjević, H.H. Bandulasena, Z.K. Nagy, Production of polymeric nanoparticles by micromixing in a co-flow microfluidic glass capillary device, *Chem. Eng. J.* 280 (2015) 316–329.
- L. Jiang, W. Wang, Y. Chau, S. Yao, Controllable formation of aromatic nanoparticles in a three-dimensional hydrodynamic flow focusing microfluidic device, *RSC Adv.* 3 (39) (2013) 17762–17769.
- R. Hood, W. Vreeland, D.L. DeVoe, Microfluidic remote loading for rapid single-step liposomal drug preparation, *Lab Chip* 14 (17) (2014) 3359–3367.
- F. Roffo, A.M. Ponsiglione, P.A. Netti, E. Torino, coupled hydrodynamic flow focusing (chff) to engineer lipid-polymer nanoparticles (lipons) for multimodal imaging and theranostic applications, *Biomedicines* 10 (2) (2022) 438.
- W.-Z.S. Lin, N. Malmstadt, Liposome production and concurrent loading of drug simulants by microfluidic hydrodynamic focusing, *Eur. Biophys. J.* 48 (6) (2019) 549–558.
- A. Jahn, F. Lucas, R.A. Wepf, P.S. Dittrich, Freezing continuous-flow self-assembly in a microfluidic device: toward imaging of liposome formation, *Langmuir* 29 (5) (2013) 1717–1723.
- M. Maeki, Y. Fujishima, Y. Sato, T. Yasui, N. Kaji, A. Ishida, H. Tani, Y. Baba, H. Harashima, M. Tokeshi, Understanding the formation mechanism of lipid nanoparticles in microfluidic devices with chaotic micromixers, *PLoS One* 12 (11) (2017), e0187962.
- E.L. Cussler, E.L. Cussler, *Diffusion: Mass Transfer in Fluid Systems*, Cambridge University Press, 2009.
- R.F. Ismagilov, A.D. Stroock, P.J. Kenis, G. Whitesides, H.A. Stone, Experimental and theoretical scaling laws for transverse diffusive broadening in two-phase laminar flows in microchannels, *Appl. Phys. Lett.* 76 (17) (2000) 2376–2378.
- M.V. Bandulasena, G.T. Vladislavjević, B. Benyahia, Versatile reconfigurable glass capillary microfluidic devices with lego inspired blocks for drop generation and micromixing, *J. Colloid Interface Sci.* 542 (2019) 23–32.
- A. Jahn, S.M. Stavits, J.S. Hong, W.N. Vreeland, D.L. DeVoe, M. Gaitan, Microfluidic mixing and the formation of nanoscale lipid vesicles, *ACS Nano* 4 (4) (2010) 2077–2087.
- N. Singh, et al., Self-organized wrinkling in thin polymer films under solvent–non-solvent solutions: patterning strategy for microfluidic applications, *ACS Appl. Polym. Mater.* 3 (12) (2021) 6198–6206.